Interactions between the accumulation of sediment storage and debris flow characteristics in a debris-flow initiation zone, Ohya landslide body, Japan

Fumitoshi Imaizumi[1], Yuichi S. Hayakawa[2], Norifumi Hotta[3], Haruka Tsunetaka[4], Okihiro Ohsaka[1],
5   Satoshi Tsuchiya[1]

[1]Faculty of Agriculture, Shizuoka University, Shizuoka, 422-8529, Japan
[2]Centre for Spatial Information Science, The University of Tokyo, Kashiwa, 277-0871, Japan
[3]Faculty of Life and Environmental sciences, University of Tsukuba, Tsukuba, 305-8572, Japan
[4]Graduate School of Life and Environmental sciences, University of Tsukuba, Tsukuba, 305-8572, Japan

10   *Correspondence to*: Fumitoshi Imaizumi (imaizumi@shizuoka.ac.jp)

Abstract. Debris flows often occur in steep mountain channels, and can be extremely hazardous as a result of their destructive power, long travel distance, and high velocity. However, their characteristics in the initiation zones, which could possibly be affected by temporal changes in the channel topography associated with sediment supply from hillslopes and the evacuation of sediment by debris flows, are poorly understood. Thus, we studied the interaction between the flow characteristics and the topography in an initiation zone of debris flow at the Ohya landslide body in Japan using a variety of methods, including a physical analysis, a periodical terrestrial laser scanning (TLS) survey, and field monitoring. Our study clarified that both partly and fully saturated debris flows are important hydrogeomorphic processes in the initiation zones of debris flow because of the steep terrain. The predominant type of flow varied temporally and was affected by the volume of storage and rainfall patterns. The small-scale channel gradient (on the order of meters) formed by debris flows differed between the predominant flow types during debris flow events. The relationship between flow type and the slope gradient could be explained by a simple analysis of the static force at the bottom of the sediment mass.

1 Introduction

Debris flows often occur in steep mountain channels and can be extremely hazardous as a result of their destructive power, long travel distance, and high velocity (Lin et al., 2002; Cui et al., 2011). To lower the hazard of debris flow, field monitoring have been conducted in many torrents in the world including Switzerland (McArdell et al., 2007; Berger et al., 2011b), Italy (Arattano, 1999; March et al., 2002; Arattano et al., 2012), the United States (McCoy et al., 2010; Kean et al., 2013), and China (Zhang, 1993; Hu et al., 2011). Many of these monitoring have been undertaken in the transportation zones of the debris flows, with only a few observations undertaken in their initiation zones, where the unstable sediment start to move (Berti et al., 1999;

Natural Hazards
and Earth System
Sciences
Open Access

Discussions

McCoy et al., 2012; Kean et al., 2013). Understanding of the decries-flow characteristics in the initiation zone is needed to estimation of debris-flow volume and timing in down reaches required for improvement of the debris-flow warning system.

Debris flows can be classified into various types according to their flow dynamics, solid fractions, and material types (Takahashi, 1991; Coussot and Meunier, 1996; Hunger, 2005). Multiple flows types appear even in the same torrent (Imaizumi
5 et al., 2005; Okano et al., 2012). However, in situ classification of debris flow type is mainly based on monitoring results obtained in the transportation zone. Field monitoring conducted at multiple sites along a debris flow torrent have revealed that flow characteristics (e.g., solid fraction and boulder size) and discharge change as the flow migrates downstream and is affected by erosion and deposition (Takahashi, 1991, Berger et al., 2011b; Arattano et al., 2012). Thus, flow characteristics in the transportation zone possibly differ from those in the initiation zone. In the initiation zone, flows containing an unsaturated
10 layer have also been observed during field monitoring (Imaizumi et al., 2005; Imaizumi et al., 2016b). Such information is needed to explain the sequence of debris flow processes from initiation in the headwaters to termination at the debris flow fan.

The topography along debris flow torrents reflects the characteristics of a debris flow event (Whipple and Dunne, 1992; Coussot and Meunier, 1996; Imaizumi et al., 2016a). The curvature of the terrain can be used to determine the relationship between shear stress and shear strength (Staley et al., 2006). Many observations of the relationships between topography and
15 flow characteristics have been made in the lower part of the debris flow torrents, while such findings are limited in the debris-flow initiation zone. In many cases, the channel gradient in the initiation zone is greater than 20° (VanDine 1985; Pareschi et al. 2002; McCoy et al., 2013; Hürlimann et al., 2015). In terms of debris flows caused by the transportation of loose sediment on the floor of a valley, both the volume and grain size of debris flow material (e.g., channel deposits and talus slope) change over time in association with the sediment supply from hillslopes, as well as the evacuation of sediment by debris flows and
20 fluvial processes (Bovis and Jakob, 1999, Imaizumi et al., 2006, Berger et al., 2011a). Although some previous studies have investigated the relationship between characteristics of the debris flow material and initiation condition of a debris flow (Bovis and Jakob, 1999; Jakob et al., 2005; Schlunegger et al., 2009; Chen et al., 2012), only a few have considered the relationship between flow material and flow characteristics (Kean et al., 2013; Imaizumi et al., 2016b). The difficulty in monitoring debris flows in steep and dangerous initiation zones has prevented the collection of the field data needed to clarify the relationship
25 between flow characteristics and flow material.

In the debris-flow initiation zone at the Ichinosawa catchment within the Ohya landslide, Japan, field monitoring has been undertaken since 1998 (Imaizumi et al., 2005; Imaizumi et al., 2006). This site is suitable for monitoring because of the high debris-flow frequency (about three or four events per year) that occur due to the mobilization of storage (i.e., talus cone and channel deposits) around the channel. In addition, detailed topographic measurements by terrestrial laser scanning (TLS) have
30 been undertaken periodically since 2011 (Hayakawa et al., 2016).

In this study, we investigated the relationship between the slope gradient and type of sediment transport based on a simple analysis of the static force. Then we considered the relationship between the accumulation conditions of storage (i.e., slope gradient and volume of storage) and debris-flow characteristics based on field monitoring results in the Ohya landslide. Our specific objectives were to explain the relationship between topography and sediment transport type by simple models, clarify

Natural Hazards
and Earth System
Sciences
Discussions

Open Access
EGU

temporal changes in the channel topography of the debris-flow initiation zone due to the occurrence of debris flows, and clarify the interaction between the characteristics of sediment storage (i.e., volume and slope gradient) and debris-flow type.

2 Slope gradient and type of sediment transport

In this section, we describe our analysis of the balance of static force at the bottom of a sediment mass to assess the relationship between slope gradient and the type of sediment transport. Shear stress at the bottom of a sediment mass needs to exceed shear strength for the initial movement of a stable mass (Takahashi, 1991; Imaizumi et al., 2016c). Similarly, shear stress needs to exceed shear strength at the bottom of a traveling sediment mass for the continuity of travel (Takahashi, 1991; Watanabe, 1994). Under the assumption that cohesion is negligible, shear stress τ and shear strength τ_r at the bottom of sediment mass can be given as follows:

$$\tau = \{(1 - \eta_w)[(1 - n)\gamma_s + nS\gamma_w] + \eta_w[(1 - n)\gamma_s + n\gamma_w]\}\sin\alpha, \tag{1}$$

$$\tau_r = \{(1 - \eta_w)[(1 - n)\gamma_s + nS\gamma_w] + \eta_w[(1 - n)(\gamma_s - \gamma_w)]\}\cos\alpha\tan\phi, \tag{2}$$

where η_w is the ratio of the depth of the saturated zone ($h_w - z_1$) to the depth of the sediment mass ($h - z_1$), h_w is the height of the water table, z_1 and h are the height at the bottom and surface of the sediment mass, respectively, n is the porosity of sediment, γ_s is the force of gravity acting on a unit volume of sediment, γ_w is the force of gravity acting on a unit volume of water (or interstitial water for debris flow), S is the degree of saturation in the unsaturated zone, α is the slope gradient, and ϕ is the effective internal angle of friction (Fig. 1). Note that α is the slope gradient of the potential sliding surface when we consider the initial movement of the stable mass, whereas it is the gradient of the surface topography when we consider the migration of the traveling sediment mass. The n in the moving sediment mass is similar to that of stable sediment when dispersion of the sediment particles is not significant, while n in the moving sediment mass greatly exceeds that of the stable sediment when the particle dispersion associated with collision among the particles is significant (e.g., fully saturated debris flow). Based on Eqs.(1) and (2), the critical condition for the movement of sediment mass ($\tau_r = \tau$) can be given as follows (Imaizumi et al., 2016c):

$$\frac{\tan\alpha}{\tan\phi} = \frac{(1 - \eta_w)[(1 - n)\gamma_s + nS\gamma_w] + \eta_w[(1 - n)(\gamma_s - \gamma_w)]}{(1 - \eta_w)[(1 - n)\gamma_s + nS\gamma_w] + \eta_w[(1 - n)\gamma_s + n\gamma_w]}. \tag{3}$$

Based on the η_w, three typical sediment transport types were considered: fully unsaturated ($\eta_w = 0$), partly saturated ($0 < \eta_w < 1$), and fully saturated ($\eta_w = 1$). In case of $\eta_w = 0$, Eq. (3) is expressed as:

$$\tan\alpha = \tan\phi, \tag{4}$$

If the slope gradient $\tan\alpha$ exceeds $\tan\phi$, the sediment mass can move without any saturation (Fig. 1a). In other words, Eq. (4) expresses the lowest boundary of the slope gradient for the movement of the fully unsaturated sediment mass (hereafter referred to as α_1). There are several types of sediment transport in fully unsaturated conditions, such as rockfall, dry granular flow, and dry ravel, which is the gravitational transport of ground surface materials by bouncing, rolling, and sliding (Carson, 1977;

Natural Hazards
and Earth System
Sciences

Open Access

Discussions

EGU

Dorren, 2003; Gabet, 2003). Although physical mechanisms between individual particles (i.e., rockfall and dry ravel) and flows of grains (i.e., dry granular flow) are different in terms of the interactions among particles, the slope gradient of talus slopes, which are formed by fully unsaturated sediment transport processes, are usually similar or slightly smaller than ϕ regardless of the transport type (Kirkby and Statham, 1975; Carson, 1977; Mangeney et al., 2007). Pyroclastic flow, which is

5 a fluid composed of a mixture of air and particles, is the exception in the above relationship between α and ϕ. Pyroclastic flow sometimes reaches terrain much smaller than ϕ (Yamashita and Miyamoto, 1993; Takahashi and Tsujimoto, 2000). The pyroclastic flow is an important sediment transport process in areas with many fine particles (i.e., volcanic areas). In this study, we did not consider pyroclastic flow because we focused on sediment transport processes in areas in which gravel, cobbles, and boulders dominated the debris flow material.

10   The relationship between slope gradient and the volumetric sediment concentration $(1 - n)$ in a saturated sediment mass is given by substituting 1 into η_w in Eq. (3):

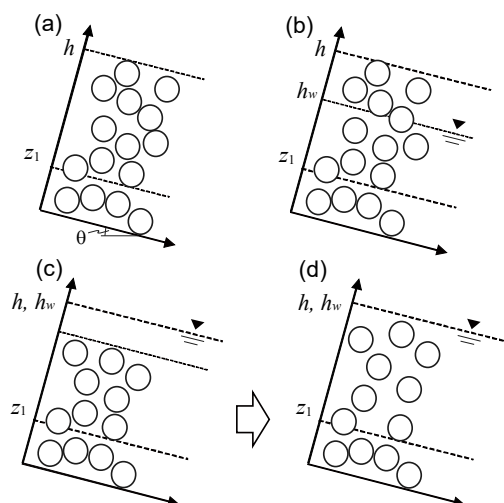$$\tan\alpha = \frac{(1 - n)(\gamma_s - \gamma_w)}{(1 - n)\gamma_s + n\gamma_w}\tan\phi.$$

(5)

Note that n here becomes larger than the n of storage when sediment particles start to disperse by collision with other particles.

15 Equation (5) expresses the relationship between the solid concentration in the steady-state flow (called equilibrium concentration) and the slope gradient (Takahashi, 1991; Egashira et al., 2001, Takahashi, 2014). A similar trend as in Eq. (5) was also found in the *in situ* measurements of Navratil et al. (2013). By substituting the porosity of the storage into n, Eq. (5) expresses the slope gradient needed for the entrainment of a fully saturated sediment mass, with no dispersion of particles (hereafter referred to as α_2). When the slope gradient of the terrain ranges between α_1 and α_2, the transportation of a partly

20 saturated sediment mass occurs (Fig. 1b) (Watanabe, 1994; Imaizumi et al., 2005; Imaizumi et al., 2016c). Equation (5) just considers shear strength and shear stress at the bottom of the sediment mass, but does not consider the conditions of the fluid of the sediment mass. Thus, not only the debris flow, but also the sliding of the sediment mass without any fluid and plug flow, of which the upper layer in the sediment mass is not fluid, also satisfy Eq. (5). Nevertheless, Eq. (5) is a necessary condition for any type of sediment movement with partly saturated conditions. Partly saturated sediment transport has also been observed

25 in channels gentler than α_2 (i.e., channel gradient < 10°) (McArdell et al., 2007; McCoy et al., 2010; Okano et al., 2012). However, the appearance of partly saturated sediment transport in such gentler channels is generally limited at the front of a surge. In torrents gentler than α_2, the existence of surface flow over debris flow material is theoretically required for the initiation of debris flow (Fig. 1c) (Takahashi, 1991; Imaizumi et al., 2016c). Once sediment starts to move, it spreads throughout the flow (Fig. 1d). Thus the volumetric solid concentration is lower than that in sediment storage $(1 - n)$.

30   The explanations above are also applicable to the relationship between the amount of water in the sediment mass from the upper channel reaches (and slopes) and the slope gradient of the terrain formed by that sediment mass (Takahashi, 1991; 2014). If the amount of water in the sediment mass from the upper channel reaches is constant, the slope gradient of the terrain

approaches the gradient given by the substitution of η_w, n, and S of the sediment mass into Eq. (3) as a result of deposition and erosion.

In this study, we call any partly and fully saturated sediment transport processes as partly and fully saturated debris flows, respectively. Although some sediment transport processes at our monitoring site were not typical debris flows, such as those composed of a mixture of sediment and water (Takahashi, 1991; Coussot and Meunier, 1996), we believe the processes at our study site directly or indirectly contributed to the initiation of debris flow.

Figure 1: Schematic diagram of sediment transport types: (a) dry (fully unsaturated), (b) partly saturated, (c) surface flow over sediments, which triggers fully saturated sediment transport, (d) fully saturated sediment transport.

3 Study site

We conducted field monitoring within the Ohya landslide in the Southern Japanese Alps (Fig. 2). The Ohya landslide has an estimated total volume of 120 million m³, and was initiated during an earthquake in A.D. 1707 (Tsuchiya and Imaizumi, 2010). The climate at the site is characterized by a high annual precipitation (about 3,400 mm) (Imaizumi et al., 2005). Heavy rainfall (i.e., total rainfall > 100 mm) occur during the rainy season from June to July and the autumn typhoon season (from August to October). The geological unit is Tertiary strata, which is composed of well-jointed sandstone and highly fractured shale. Unstable sediments have been supplied from outcrops into the channels in the landslide scar and have affected the initiation of debris flows since the original failure.

Almost all of debris flows in the Ohya landslide occur in the upper Ichinosawa catchment (Imaizumi et al., 2005). The total length of the channel is ≈650 m and the south-facing catchment (1,450 – 1,905 m a.s.l) has an area of 0.22 km^2. Most of the basin is characterized by high and steep slopes (40 – 65°). Seventy percent of the slope is scree and outcrop, whereas the remaining 30% is covered with forest, shrubs, and tussocks. Anthropogenic influences are absent in the catchment because of

5   the harsh environmental conditions.

Unconsolidated debris, ranging from sand particles to boulders (Imaizumi et al., 2016c), is located in the channel bed and talus cones, and is the source of debris flow material (Imaizumi et al., 2006). The thickness of debris deposits, including large boulders (> 1 m), exceeds several meters in some sections. Freeze-thaw that promotes dry ravel and rockfalls are the predominant sediment infilling of the channels (Imaizumi et al., 2006). Most of the channel was covered by channel deposits

10   when a large volume of storage accumulated in the bottom of the valley, while the channel bed is alternatively composed of bedrock and sediments when the storage volume is low. Volume of storage displays seasonal changes caused by sediment supply from hillslopes in winter and early spring, and the evacuation of storage due to the occurrence of debris flow in summer and autumn (Imaizumi et al., 2006). The stored sediment has never been completely eroded by debris flows. Changes in the volume of storage at longer time scales (several years) occurs by the timing of large debris flows with a volume > 15,000 m^3

15   that drastically decrease volume of storage (Imaizumi et al., 2016c).
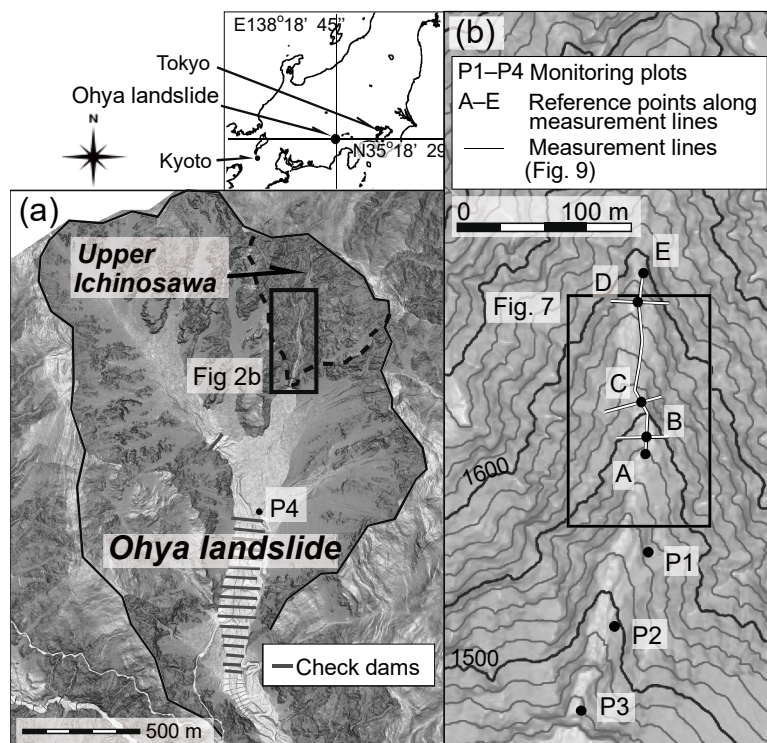
Figure 2: Map of the Ohya landslide and upper Ichinosawa catchment: (a) Ohya landslide, (b) Ichinosawa upper catchment. Gentler and steeper terrains are expressed as light and dark colors, respectively.

4 Methodology

5   **4.1 Debris-flow Monitoring**

The monitoring system was installed in the study site in spring 1998 and consisted of a rain gauge, ultrasonic sensors, water pressure sensors, and a video camera (Imaizumi et al., 2005). The video camera, which provided motion images of debris flows, was initially monitored at P4, then moved to P2 in 2000 (Fig. 2a). During the period of 1998 to 2001, the video camera was programmed to take 0.75 s clips of video every 5 min. In April 2001, this interval was shortened to 3 min to capture flow

10   characteristics in more detail. In addition, continuous monitoring cameras, of which recording was initiated by wire motion sensors installed at several cross-sections in the channel, were initially installed at P1 in 2003, then at P3 and P2 in 2004 and 2005, respectively. The video camera system sometimes failed to capture debris flows because of their mechanical problems due to harsh site conditions. We identified timing of such debris flows by field surveys and water pressure sensors. Flow depth

and surface velocity of debris flows at 1 second intervals were obtained from video image analysis. The surface velocity provided by the video image analysis does not represent the mean velocity of all layers of the flow. The mean velocity was estimated from surface velocity multiplied by 0.6, based on the velocity profile throughout the flows on movable beds obtained from a physically based model by Takahashi (1977, 2014). Changes in cross-sectional area of flow were calculated from

5   changes in flow depth and cross-section measurement of the channel topography. Discharge of debris flows were estimated from the cross-section area multi-plied by mean velocity of all layers.

Imaizumi et al. (2006) classified the flow phases during debris flow events into two primary types: flows that made of mainly muddy water and those made of mainly cobbles and boulders. The former flows are turbulent and are characterized by black surfaces due to high concentrations of silty sediment sourced from shale in the interstitial water (Fig. 3a). Because the

10   matrix of boulders is filled with interstitial water, this flow is considered fully saturated (Fig. 1d). In contrast, muddy water is not identified in the matrix of the flow surface of the second type of flow (Fig. 3b). Therefore, this type of flow is considered partly saturated (Fig. 1b). We visually identified temporal changes in the flow type during debris flow events from video images based on the existence of interstitial water on the flow surface.

Time-lapse cameras (TLCs; GardenWatchCam, Brino, Taipei City, Taiwan) were installed around P1 and P2 in April, 2013,

15   as a backup for video camera monitoring. The number of cameras (1 to 6) differed among the various measurement periods. The intervals used for capturing images were also different among the measurement periods and for the various cameras, with a range from 1 s to 10 min.

To identify the arrival of debris flow, a semiconductor type water pressure sensors, which monitored hydrostatic pressures up to 49 kPa with an accuracy of ± 3%, were placed in holes dug in the bedrock of the channel bed. The logging interval was

20   set at 1 min. Because water pressure sensors were sometimes washed away by debris flow, ultrasonic sensors with a measuring range from 120 to 600 cm (accuracy of ± 0.4%) were installed to monitor the surface height of debris flows at 1 min intervals as the backup of water pressure sensors. Water pressure and flow height monitored by these instruments showed intense and abrupt changes during the passage of debris flows, whereas such changes were absent during rainfall-runoff events without occurrence of debris flow. Therefore, we used water pressure and flow depth to identify the occurrence of debris flows.

Natural Hazards
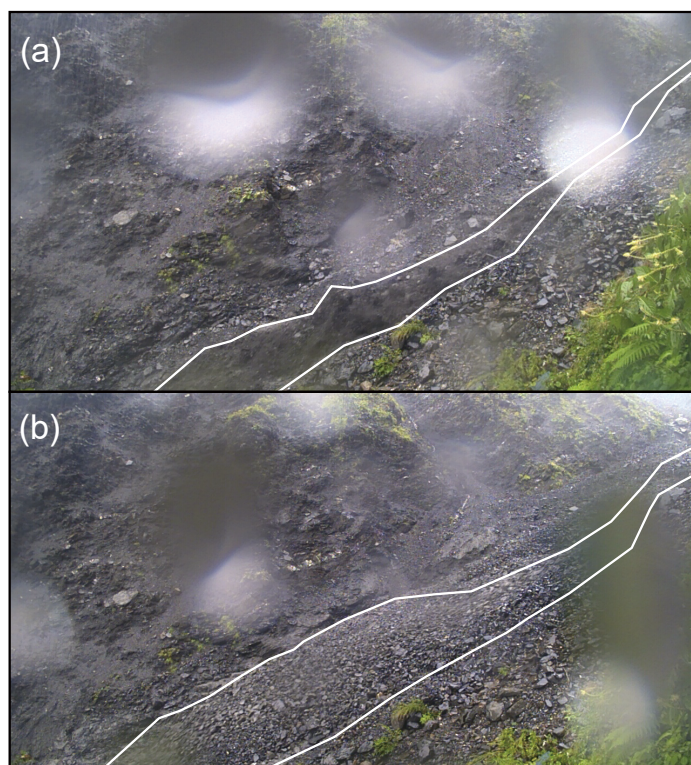and Earth System
Sciences

Open Access

Discussions

EGU

Figure 3: Images of fully and partly saturated debris flows captured by a TLC at plot P2 in Fig. 2. (a) Fully saturated debris flow captured 9 September 2015, 8:41 (LT). (b) Partly saturated debris flow captured at 9 September 2015, 7:43 (LT). Cobbles and boulders covers flow surface of the partly saturated debris flow (Imaizumi et al., 2016b).

5

4.2 Topographic Data Obtained by TLS

To clarify temporal changes in the micro channel bed topography associated with occurrence of debris flows, a TLS unit (GLS-1500 Topcon Co., Tokyo, Japan) was used to measure the topography of valley axis (Fig. 2) (Hayakawa et al., 2016). The maximum measurable distance of the TLS unit is 500 m (for target objects with a 90% reflectance), with accuracies of 6" for

10 angle and 4 mm for distance (at 150 m range). From November 2011, field measurements were undertaken in spring, summer, and autumn for 4 years (Table 1). For each measurement, the scanner was set at two positions. One was at the downstream side of the target area (P1 in Fig. 2), where the land had been relatively stable for many years. The other at the upstream side of the target area (around point D in Fig. 2). The location of this scan position varied because it was in the valley bottom where

Natural Hazards
and Earth System
Sciences
Discussions

the topography changed significantly due to debris flows. The point clouds measured from different scan positions were registered using at least five reference targets placed between the two scan positions. The two point clouds were registered by the target matching method using these reference targets, with accuracies of 0.5–6 mm. The geographic coordinates (Japan Plane Rectangular CS VIII, EPSG: 2450) of two targets, selected as georeference points, were measured with global navigation

5   satellite system (GNSS) receivers (GeoXH 6000, Trimble, Sunnyvale, CA, USA or GRS-1, Topcon Co., Japan; accurate to a range of 10–63 mm in XY or Z). The baseline solution was calculated using data from GNSS base stations of GEONET, the Japanese GNSS network operated by the Geospatial Authority of Japan. The overall uncertainties of the point clouds, including scanning, registration, and georeferencing by GNSS, were considered in the order of centimeters to a decimeter (Hayakawa et al., 2016).

10

Table 1: Date of TLS survey

Year	Date of survey	Number of debris flow after previous scanning	Date of last debirs flow event[*1]
2011	November 11	-	October 14
2012	May 14	0	-
	August 23	3	July 13
	November 21	3	September 30
2013	May 10	0	-
	August 16	0	-
	November 19	2	September 15
2014	May 16	0	-
	August 17	1	August 10
	November 28	2	October 5
2015	May 15	0	-
	August 23	4	August 17
	December 4	2	September 9

*1 Date of the last debris flow event are not listed when debris flow had not occurred in the year , because the topography was possibly affected by the winter sediment supply rather than the last debris flow in the previous year.

15   After manually eliminating noise and unnecessary points, the point clouds obtained by the TLS measurement were converted into digital elevation models (DEMs) using a simple triangulated irregular network (TIN) interpolation, because vegetation cover was absent in the site. The resolution of the DEMs was set at 10 cm, which sufficiently covers the average point density of the point clouds. Areas with sparse point clouds (approximately <100 point m^{-2}), vegetated areas, and areas affected by the combination of various processes (e.g., talus slopes with the lower part eroded by stream flow) were excluded from the analyses.

20   The extent of typical geomorphic units in the TLS survey area, including three rock slopes, three talus slopes, and a channel around the monitoring plot P1, was mapped by field surveys to calculate the slope gradient of geomorphic units with various grid sizes (Fig. 4). The mapping was conducted at the same time as each TLS survey because the area changed over time due to the sediment supply from outcrops and transportation of sediment by debris flows.

Figure 4: Photograph of the typical geomorphic units seen from P1. The image shows the area of rock slopes (surrounded by red lines), talus slopes (surrounded by yellow lines), and a channel (surrounded by blue lines), for which the slope gradient was calculated from DEMs with various grid sizes. The numbering of the area corresponds to that used in Fig. 7.

4.3 Estimation of debris-flow volumes

5   We estimated the volume of storage from photographs taken periodically at sites P1 and P4 (Fig. 2) (Imaizumi et al., 2016a). We could not use data obtained by periodical TLS, because the target area of the TLS was a fraction of the storage zone. Photographs from site P4 cover the entire study site, whereas those from P1 focus on channel deposits at the bottom of the incised main channel, which is shaded in photographs from P4. The area covered by channel deposits and talus slopes in each photograph periods was mapped on GIS based on these photographs. The bedrock topography in the upper Ichinosawa

10   catchment was estimated from terrains by airborne laser scanning (ALS) in the periods when sediment storage was almost absent (i.e., in 2011 and 2012). Thirty-three cross-sectional areas of the storage with spacing of 25 m along the channels (24 cross-sections along the main channel and 9 cross-sections along a tributary) were calculated from the bedrock topography and the location of both ends of the storage along the cross-sections on the GIS storage map under the assumption that surface topography of the storage was an inclined line connecting both ends of the storage. Total volume of the storage was calculated

15   by sum of the cross-sectional area multiplied by the spacing of cross-sections (25 m). The root mean squared error (RMSE) of the procedure, which was obtained from comparison of the volumes of storage by the procedure and that by subtraction of ALS DEMs by estimated bedrock topography, was 5361 m^3 (Imaizumi et al., 2016a). This RMSE is larger than the volume of small debris flows (<2000 m^3) but below the sediment supply volume in each year (>10,000 m^3).

11

Natural Hazards
and Earth System
Sciences

Open Access

EGU

Discussions

5 Results

5.1 Debris flow monitoring

From 1998 to 2015, 59 debris flows, which went through or terminated in the section between sites P1 to P3, were observed by video cameras, field surveys, and water pressure sensors in the upper Ichinosawa catchment. In addition, the occurrence of

5   some other debris flows, which terminated above site P1, were found by periodic photography and field surveys. We analyzed video images of seven flows that were clearly captured by video cameras. In addition, we analyzed photographs of one debris flow taken by TLCs with an interval of 1 s (Table 2). We failed to obtain clear video images of other debris flows because of darkness at night and fog. Most of the rainfall events triggering debris flows in the study site can be classified into two groups: long-lasting rainfall events with high total rainfall, caused by typhoons and stationary fronts (rainfall duration >5 h and total

10   rainfall >50 mm), and short-duration convective rainfall events of high intensity (rainfall duration <5 h, total rainfall <50 mm; Table 2).

As noted above, two types of flow have been observed in the Ohya landslide: flow mainly composed of cobbles and boulders (partly saturated flow) and flow mainly composed of muddy water (fully saturated flow). The duration of each flow phase differed between events. For example, a large part of the debris flow surges (88% in terms of total duration) was composed of

15   partly saturated flow during a debris-flow event on 5 August 2008, while 90% in terms of the total duration of surges was classified as fully saturated flow during a debris-flow event on 30 August 2004 (Fig. 5). Although the camera locations, which could potentially affect flow characteristics, differed among events, the proportional duration of the partly saturated debris flow in overall debris flow surges had a weak positive relationship with the volume of storage estimated from periodical photography ($R^2 = 0.37$, p-value = 0.06; Fig. 6). Rainfall was also a potential factor controlling flow type. The duration of

20   fully saturated flow as a proportion of the whole debris flow surges was generally high during long-lasting rainfall events associated with typhoons and stationary fronts, while the duration of partly saturated flow as a proportion of the whole surges was high during convective rainfall events of short duration (Fig. 6, Table 2). The p-value for the difference in the duration of the different flow types between the two rainfall patterns was below 0.01.

Natural Hazards
and Earth System
Sciences
Discussions

Table 2: Details of the rainfall and flow types during the debris flow events analyzed in this study

Date	Total rainfall (mm)	Maximum 10-min. rainfall intensity (mm/10min.)	Rainfall duration	Rainfall type	Type of camera	Location of camera	Proportional duration of partly saturated flow in overall debris flow surges
30 August 2004	276.5	7.5	31 h 50 min.	Typhoon	Video	P3	0.10[*a]
19 July 2006	178.0	5.5	37 h 10 min.	Stationary front	Video	P2	0.65
6 September 2007	501.5	9.5	37 h 30 min.	Typhoon	Video	P2	0.49[*a]
5 August 2008	39.5	13.5	1 h 30 min.	Convective	Video	P2	0.88
24 July 2010	21.0	13.0	1 h 10 min.	Convective	Video	P2	1.00
30 September 2012	86.0	6.5	7 h 40 min.	Typhoon	Video	P3	0.23[*a]
6 August 2015	44.5	21.0	1 h 50 min.	Convective	Video	P1	0.99
9 September 2015	203.0	8.0	36 h 50 min.	Typhoon	TLC	P1	0.42

[*a] Latter half of the debris flow event was not analyzed because of the darkness affected by the sunset. Therefore, latter half of the event is not included in this data.
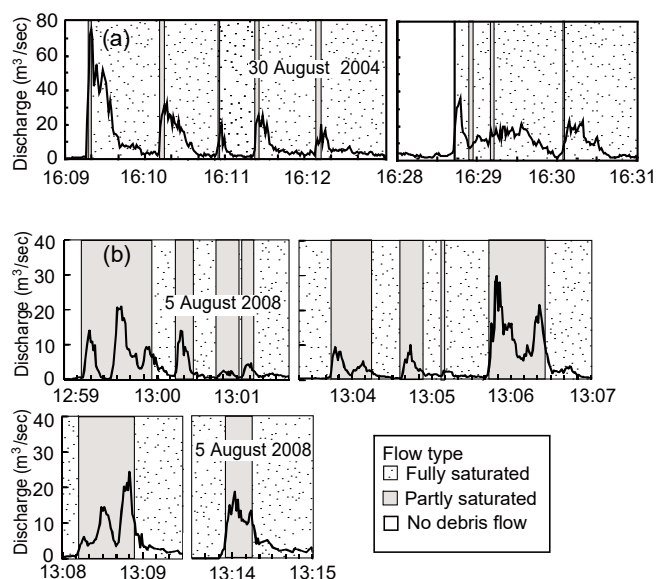

Figure 5: Hydrograph and the duration of each flow type during debris flow events. (a) Debris flow on August 30, 2004, mainly consisting of fully saturated flow. (b) Debris flow on August 5, 2008, mainly consisting of partly saturated flow.
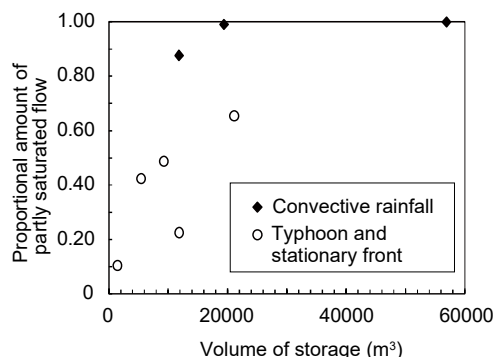
5

Figure 6: Comparison between the volume of storage and the duration of partly saturated flow as a proportion of the overall debris flow surges.

5.2 Slope gradient of geomorphic units

5   Mapping of the three geomorphic units (rock slopes, talus slopes, and the channel) in the TLS survey area showed that the location of each unit was largely similar throughout the study periods, while the size of each unit changed due to sediment supply and transport processes. Some talus slopes completely disappeared in several periods because of erosion by debris flows. The roughness of the ground surface attributable to boulders, at a scale on the order of decimeters (Imaizumi et al., 2016c), was clearly visible on the slope gradient map, with a grid size of 0.1 m obtained by TLS (Fig. 7). Step-pool-like

10   topography with a height of several meters formed by large boulders (>1.0 m) and bedrock morphology was visible in the channel on the slope gradient maps with a grid size of ≥1.0 m (Fig. 7).

   Average and standard deviation of slope gradient in the three geomorphic units (rock slopes, talus slopes, and the channel) throughout the TLS monitoring period were calculated from DEMs with various grid size. Regardless of the grid size, the average slope gradient of rock slopes and the channel were highest and lowest among the three geomorphic units, respectively

15   (Fig. 8a). The average slope gradient of each geomorphic unit becomes gentler with an increase in the grid size (Fig. 8a). However, the relationship between grid size and slope gradient was slightly different among geomorphic units. For a grid size of ≥1.0 m, a histogram of talus slopes was concentrated in a narrow range around the average value (i.e., >60% in the range between 34–40° for a grid size of 5.0 m; Fig. 8b). This slope angle is considered to represent α_1, as reported in previous studies (Kirkby and Statham, 1975; Carson, 1977; Obanawa and Matsukura, 2008). Wide distribution of the slope gradient for a grid

20   size < 1.0 m was mainly attributed to the roughness of the topography by cobbles and boulders. The standard deviation of the slope gradient in the rock slope decreased with an increase in grid size when the grid size was smaller than the width of alternative strata in the study area (about 4.0 m; Imaizumi et al., 2015), and was almost constant when the grid size was larger than that. The standard deviation of the slope gradient in the channel also decreased with an increase in grid size when the grid

size was smaller than 4.0 m, and was almost constant when the grid size was larger than 4.0 m. This inflection point of the

trend (4.0 m) was probably affected by the largest boulder size in the channel (Imaizumi et al., 2006; Imaizumi et al., 2016c).
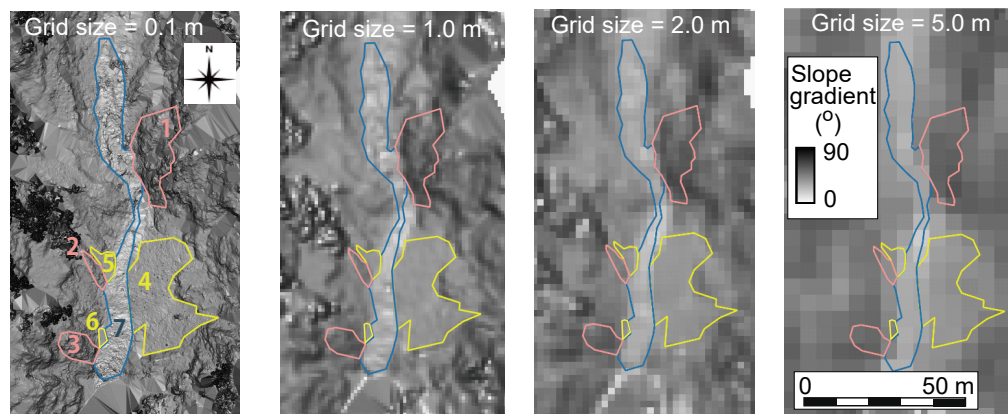

Figure 7: Slope gradient map calculated from terrestrial laser scanning (TLS) data on 14 May 2014, with various grid sizes. The
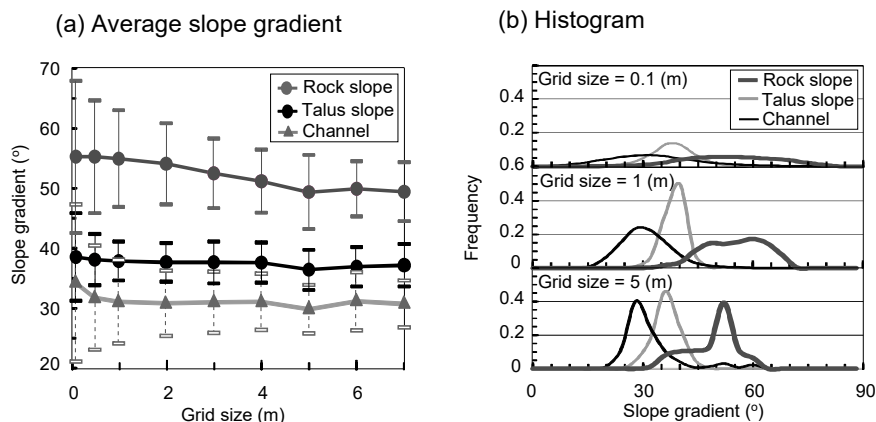5   **location of the analysis area is shown in Fig. 2.**

Figure 8: Slope gradient of typical geomorphic units calculated from terrestrial laser scanning (TLS) derived digital elevation maps
(DEMs) with various grid sizes. Topographic data in all measurement periods were used in the statistical analysis. (a) Changes in
the average slope gradient of each geomorphic unit with an increase in the grid size. The slope gradient in all periods was averaged.
10   **The bars attached to the plots indicate the range of the standard deviation. (b) Histogram of the slope gradient calculated from TLS**
DEMs, with grid sizes of 0.1, 1.0, and 5.0 m.

Natural Hazards
and Earth System
Sciences

Open Access

EGU

Discussions

5.3 Longitudinal channel topography

To clarify the effects of debris flow type on the characteristics of the channel topography, temporal changes in the longitudinal channel profiles were analyzed in the section between points A and E (total length of 100 m; Fig. 2). The channel topography on 21 November 2012 was mainly formed by a debris flow on 30 September 2012, which was dominated by fully saturated
5   flow (Fig. 8). In contrast, the channel topography on 23 August 2015, was mainly formed by a debris flow on 6 August 2015, which was dominated by partly saturated flow. A small debris flow on 17 August 2015, which transported storage with a volume of <3,000 m^3, also affected a part of the channel topography measured on 23 August 2015; however, the affected area was limited (mostly a width of <5 m) because of its small discharge.

As reported by Hayakawa et al. (2016), the channel bed deformation differed between channel sections (Fig. 9a). When we
10   compared channel bed profiles on 21 November 2012, and 23 August 2015, the channel bed level was clearly different (>3 m in depth) in the sections within 25 m and from 75 to 90 m upstream of point A. In contrast, there was almost no change in the longitudinal channel profile (<1 m) in the section within 30 m upstream of point C. Such differences in channel bed deformation could also be identified in the cross-sectional profile. The cross-sectional profile at points B and D was clearly different, while difference in the profile was not apparent at point C (Figs. 9e, 9f, 9g).
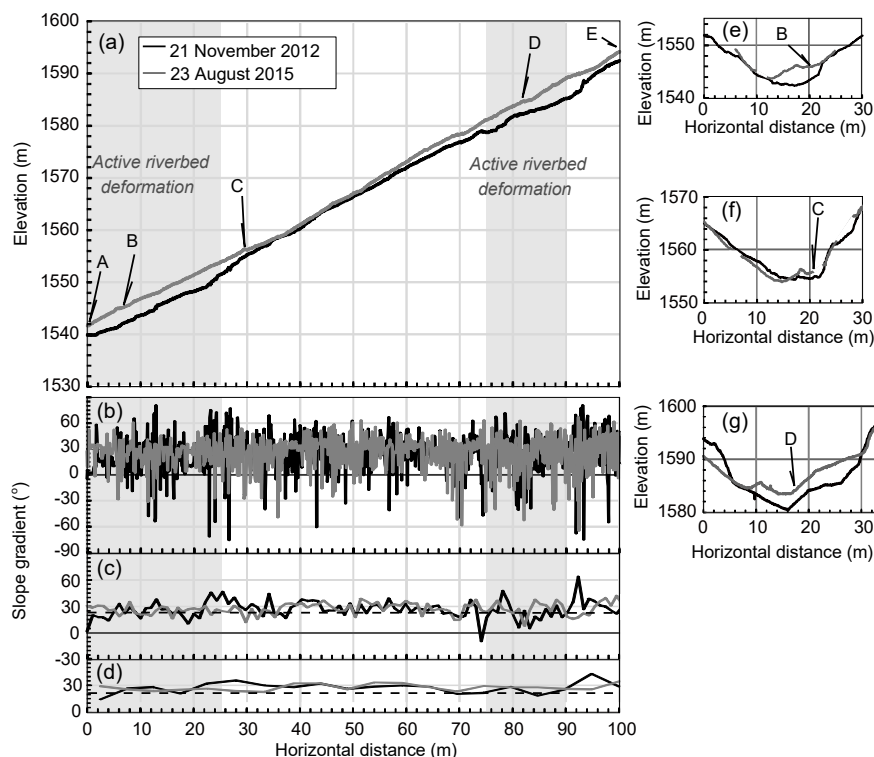
15   The longitudinal profile of the channel gradient differed among debris flow events. The distribution of the channel gradient calculated for each 0.1 m section (the scale of a boulder) on November 21, 2012 (mainly formed by fully saturated flow), was clearly wider than that on 23 August 2015 (mainly formed by partly saturated flow; Fig. 9b, Table 3a). The p-value obtained by an F-test of the difference in the dispersion of the channel gradient between the two periods was <0.001. In contrast, the average slope gradient in the section between A and E was not significantly different between the two periods (23.1° and 25.4°
20   for 21 November 2012, and 23 August 2015, respectively).

The difference in the amplitude of the channel gradient calculated for each 1.0 and 5.0 m section was also clear (Figs. 9c, 9d, Table 3a). The p-values obtained by an F-test of the difference in the dispersion of the channel gradient between the two periods was <0.001 and <0.05 for each 1.0 and 5.0 m section, respectively. Such temporal changes in the channel gradient was more evident in the sections with active channel bed deformation (from 0 to 25 and from 75 to 90 m from point A) compared
25   to those without active channel bed deformation (from 25 to 75 and from 90 to 100 m from point A) (Tables 3b, 3c). Wide distribution of the slope gradient for each 5.0 m section on 21 November 2012 was mainly attributed to the step-pool topography formed by large boulders and the bedrock step-pool, while that for each 1.0 m section was attributed to such small-scale topographies together with the particle size of large boulders.

Periodic photography and field surveys after eight debris flows, which were successfully monitored by video cameras and
30   TLCs, indicated that small-scale topography after debris flows mainly consisting of fully saturated flow are rugged compared to that after debris flows mainly consisting of partly saturated flow. This trend agrees with that observed by TLS surveys (Fig. 9, Table 3a).

Natural Hazards
and Earth System
Sciences

Discussions

The standard deviation of the channel gradient in the active channel bed deformation sections had a negative relationship with the volume of the storage (Fig. 10a). The p-values for the linear regressions with section lengths of 0.1, 1.0, and 5.0 m were <0.1, <0.05, and <0.05, respectively.

Figure 9: Channel profiles and channel gradient mainly formed by fully saturated flow (measured on 21 November 2012) and partly saturated flow (measured on 23 August 2015), obtained from 0.1 m terrestrial laser scanning (TLS) derived digital elevation maps (DEMs). (a) Longitudinal channel profile in the section between A to E in Fig. 2. (b) Longitudinal changes in the channel gradient calculated for each section with a length of 0.1 m. (c) Longitudinal changes in the channel gradient calculated for each section with a length of 1.0 m. (d) Longitudinal changes in the channel gradient calculated for each section with a length of 5.0 m. (e) Cross-sectional profile of the channel at point B. (f) Cross-sectional profile of the channel at point C. (g) Cross-sectional profile of the channel at point D. Data at some cross-sections on 9 August 2015, are absent because of the failure of the TLS survey due to the weather conditions (panels e and f).

Natural Hazards
and Earth System
Sciences

Discussions

Open Access

EGU

Table 3 Standard deviation of the channel gradient and proportional amount of channel sections in which the gradient was in the range between α_2 and α_1 throughout the entire channel section.

(a) Entire channel section between points A to E

Measurement date	Standard deviation of the channel gradient			Proportion of all sections between α_1 and α_2		
	0.1 m interval	1.0 m interval	5.0 m interval	0.1 m interval	1.0 m interval	5.0 m interval
21 November 2012	23.7	10.3	5.8	0.31	0.52	0.80
23 August 2015	18.7	7.0	3.7	0.38	0.73	0.95

(b) Sections with active channel bed deformation (from 0 to 25 and from 75 to 90 m from point A).

Measurement date	Standard deviation of the channel gradient			Proportion of all sections between α_1 and α_2		
	0.1 m interval	1.0 m interval	5.0 m interval	0.1 m interval	1.0 m interval	5.0 m interval
21 November 2012	27.0	11.4	6.3	0.30	0.38	0.44
23 August 2015	17.9	7.2	3.4	0.48	0.71	0.89

(c) Sections without active channel bed deformation (from 25 to 75 and from 90 to 100 m from point A).

Measurement date	Standard deviation of the channel gradient			Proportion of all sections between α_1 and α_2		
	0.1 m interval	1.0 m interval	5.0 m interval	0.1 m interval	1.0 m interval	5.0 m interval
21 November 2012	20.9	8.6	5.1	0.34	0.61	0.90
23 August 2015	18.8	6.5	3.5	0.33	0.76	1.00

Natural Hazards
and Earth System
Sciences
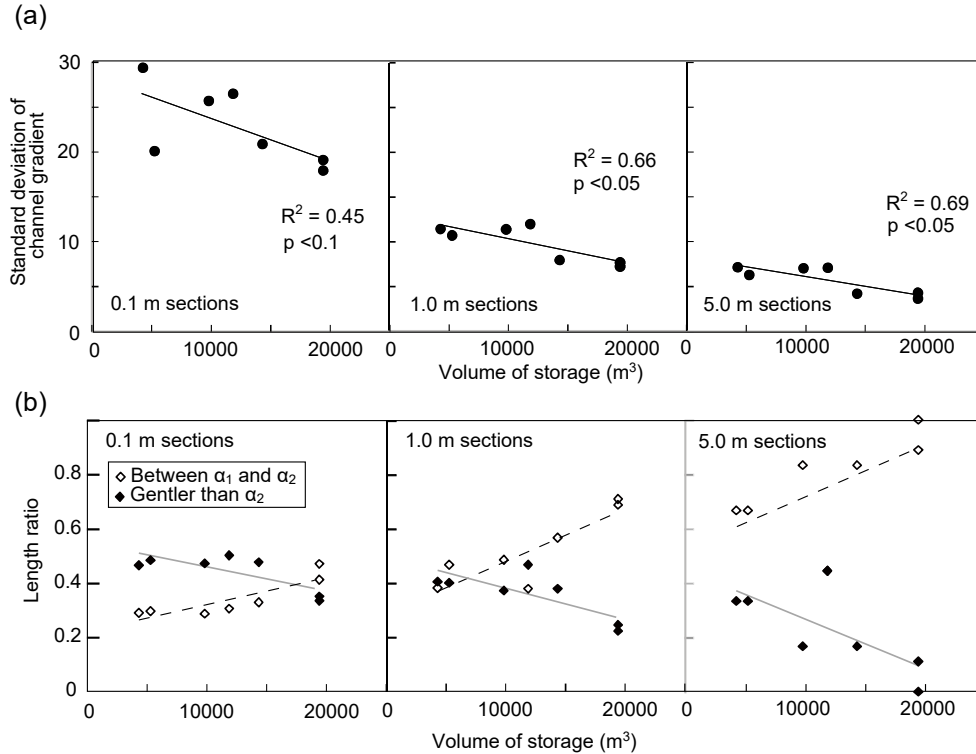Discussions
Open Access

Figure 10: Comparison between the volume of storage and channel topography. (a) Comparison of the volume of storage with the standard deviation of the channel gradient for each 0.1, 1.0, and 5.0 m section in the active channel bed deformation zones (from 0 to 25 m and from 75 to 90 m upstream of point A). (b) Comparison of the volume of storage with the length of the channel sections, in which the channel gradient ranged between α_1 and α_2 (theoretical channel gradient for partly saturated debris flow) and gentler
5 **than α_2 (theoretical channel gradient for fully saturated debris flow), in the active channel bed deformation zones. Topographic data before the first debris flow in each year were excluded from the analyses, because the channel gradient was possibly affected by the sediment supply from hillslopes, as well as the last debris flow of the previous year. The topography on August 17, 2014, was also excluded from the analysis because we failed to measure topography by terrestrial laser scanning (TLS) in the upper part of the active channel bed deformation zones because of fog. Linear regression lines for each relationship are also shown in the figure.**

10   As noted above, the theoretical channel gradient dividing partly and fully saturated debris flows (α_2) can be obtained from

Eq. (5). Because the dispersion of boulders in the partly saturated debris flows was not evident in video images, porosity (ratio

of liquid and vapor phases, to be exact) in the partly saturated flow may not be higher than that in the saturated channel deposits.

By assuming $\phi = 37.3°$ (average slope gradient of the talus slope for a grid size = 1.0 to 7.0 m), $n = 0.3$ (same as the porosity

of channel deposits), $\gamma_s = 26000$, and $\gamma_w = 9800$, the α_2 in the Ohya landslide was 22.2°. When we focused on the channel

15   sections with active channel bed deformation (from 0 to 25 m and from 75 to 90 m upstream of point A), the proportional

amount of all channel sections in which the gradient was in the range between α_2 and α_1 (theoretical channel gradient for partly

saturated flow) in the entire channel section on 23 August 2015 (mainly formed by partly saturated flow) was higher than on 21 November 2012 (mainly formed by fully saturated flow), regardless of the length of channel section used to calculate the channel gradient (Table 3b). Changes in the channel gradient were less clear in sections without clear channel bed deformation compared to those with active channel bed deformation (Table 3c).

5   The proportional amount of all channel sections, in which the gradient was in the range between α_2 and α_1, throughout the entire channel section with active channel bed deformation was higher when the volume of storage was large (Fig. 10b). The relationship was clear for all 0.1, 1.0, and 5.0 m section lengths (p-value < 0.05). In contrast, the proportional amount of all channel sections, in which the channel gradient was gentler than α_2, throughout the entire channel section decreased with an increase in the volume of sediment storage. The gradient of the regression line for the section length of 0.1 m was gentler than

10   that for the section lengths of 1.0 and 5.0 m.

6. Discussion

6.1 Factors controlling the debris flow type

In contrast to debris-flow transportation zones in other torrents, in which partly saturated flow dominates just at the front of surges (McArdell et al., 2007; McCoy et al., 2010; Okano et al., 2012), our observations in the debris flow initiation zone of

15   the upper Ichinosawa showed that partly saturated flow sometimes dominates the entire debris flow (Table 2). As with many sections in the upper Ichinosawa catchment (Fig. 9), channel gradients in the debris flow initiation zones in many other torrents are greater than 22.2° (e.g., VanDine 1985; McCoy et al., 2012), which is the theoretical channel gradient needed for a partly saturated debris flow in the Ichinosawa catchment. Although the α_2 is different among torrents affected by soil parameters such as the internal angle of friction, debris flow initiation zones in other torrents possibly satisfy the conditions for the

20   occurrence of partly saturated flow.

The proportional duration of partly saturated flow in the overall surges had a positive relationship with the volume of storage (Fig. 6). Thus, the volume of storage was a factor controlling not only the initiation of the debris flow, particularly in the supply limited basin (Bovis and Jakob, 1999; Jakob et al., 2005), but also the debris flow characteristics. The water content in the storage, which is considered an important factor controlling flow characteristics (Takahashi, 1991; Hürlimann et al., 2015),

25   may affect such relationships. When a large volume of storage is present in a basin, a large amount of water is needed for saturation of the storage, which can be difficult to attain. In such cases, even if the sediment mass that initially moved in the channel was saturated, storage along the channel eroded by the debris flow would not be fully saturated when the channel gradient >α_2. Consequently, partly saturated flow can easily dominate when a large volume of storage accumulates in the channel. Such erosion of unsaturated sediment has also been reported in other channels (Berger et al., 2011b; McCoy et al.,

30   2012). In contrast, storage can be easily saturated by smaller amounts of rainfall when there is only a small volume of storage in the basin. Thus, even when debris flows were not fully saturated in their initial stages, as they traveled downstream they easily became saturated by the water supply from tributaries as well as the erosion of saturated deposits.

Our monitoring results also revealed that the proportional duration of partly saturated flow in a debris flow event was low during long-lasting rainfall events (e.g., typhoons and stationary fronts), while the duration was high during short-lasting rainfall events (e.g., convective rainfall; Table 2, Fig. 6). The relationships between rainfall patterns and flow characteristics have also been reported in other debris flow basins (Okano et al., 2012; Kean et al., 2013; Hürlimann et al., 2014). Okano et

5   al. (2012) obtained a similar trend to that found in Ichinosawa catchment based on observations in the transportation zone. The front of a surge was completely saturated when rainfall intensity over a long duration (24 h) was high, while partly saturated flow occurred at the front of surges during short-term, intense rainfall events. Such a relationship between flow type and rainfall pattern can also be explained by the water content in the storage. During long-lasting rainfall events with high levels of cumulative rainfall, the amount of water in the storage can be high, resulting in a predominance of saturated flow. Water

10   supply from tributaries during such long rainfall events also increases the water content in the debris flow (Okano et al., 2012). In contrast, the amount of water in the storage may be low during short-duration rainfall events with low levels of cumulative rainfall, resulting in the domination of partly saturated flow.

6.2 Slope gradient of geomorphic units

The peak of the histogram for each geomorphic unit was steep and high when the grid size was sufficiently large to eliminate

15   the influence of small-scale roughness attributed to particle size (Fig. 8b). A large part of the histogram of the rock slopes was steeper than 40° for a grid size of >4.0 m (e.g., 80% for a grid size of 5.0 m; Fig. 8b), indicating that fully unsaturated sediment transport, which occurs on slopes steeper than α1 (Eq. (4)), is dominant on rock slopes. In contrast, most of the channel was gentler than α_1 for a grid size of >4.0 m (e.g., >85% for a grid size of 5.0 m; Fig. 8b), indicating that fully and partly saturated debris flows are dominant in the channel. Such a trend was also apparent in the longitudinal profile of the channel (Fig. 9b).

20   Based on the statistics of the channel gradient for each 5.0 m channel section, the sum of the length ratio of the channel sections in the theoretical range of fully and partly saturated debris flows was almost 1.0.

The longitudinal channel gradient changed with time and was affected by the predominant type of flow during the preceding debris flow events (Fig. 9). The proportional amount of channel sections between α_1 and α_2 (theoretical range of the channel gradient for partly saturated debris flow) among all active channel deformation sections was higher when a larger volume of

25   storage was present in the catchment (Fig. 10b). Because partly saturated flow dominated when a large volume of storage was present in the catchment (Fig. 6), partly saturated debris flow likely formed channel topographies with a theoretical channel gradient for the partly saturated flow (Fig. 11). Similarly, the length of the channel sections in the theoretical range for fully saturated flow ($<\alpha_2$) was high when small amounts of storage accumulated in the channel (Fig. 10b), during periods when fully saturated flow dominated (Fig. 6). Thus, fully saturated flow tended to form channel sections gentler than α_2 (Fig. 11). The

30   standard deviation of the channel gradient after a debris flow mainly consisting of fully saturated flow was higher than that after a debris flow mainly consisting of partly saturated flow (Fig. 8, Table 3). In addition, the standard deviation of the channel gradient was high when small volumes of storage accumulated in the basin (Fig. 10a), implying that fully saturated flow tended to form a step-pool topography. As a result of field surveys and periodic topography, step-pool topography formed by large

boulders and the bedrock was generally seen after fully saturated flows. Since temporal changes in the channel gradient were not apparent in the larger-scale topography (i.e., channel gradient for entire sections with an active riverbed deformation with a length of 40 m), the decrease in the channel gradient due to fully saturated flow did not occur throughout the channel but was occasionally interrupted by steep sections (Fig. 11). Periodic photography from P1 showed that the proportional amount

5 of coarse sediment generally increased after the passage of debris flows mainly consisting of saturated flow. The selective removal of fine sediment, which was monitored in the Ichinosawa catchment (Imaizumi et al., 2006; Hayakawa et al., 2016), was evident when fully saturated debris flows occurred, resulting in formation of step-pool topography by large boulders after fully saturated debris flows.

Because we did not consider the dynamic mechanisms of the debris flow, including the collision of particles and the dynamic

10 pressure of interstitial water (Coussot and Meunie, 1999; Takahashi, 2014), our analysis does not explain the unsteady nature of debris flows, such as temporal changes in the flow type during a debris flow event (McArdell et al., 2007; McCoy et al., 2013; Okano et al., 2012). Nevertheless, our analysis enables an understanding of the overall relationship between the predominant types of debris flow and slope gradient.
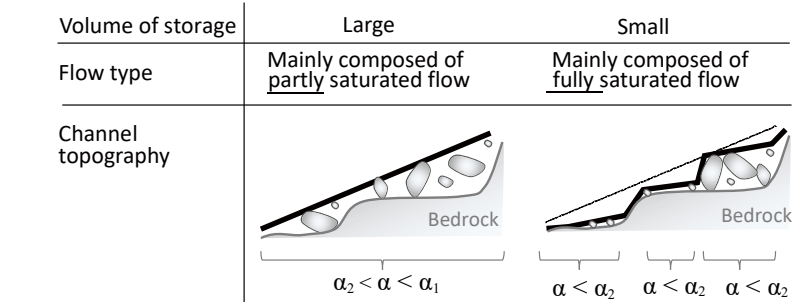
Volume of storage	Large	Small
Flow type	Mainly composed of partly saturated flow	Mainly composed of fully saturated flow
Channel topography		

15 **Figure 11: Schematic diagram of the relationships between the volume of storage, flow type, and channel topography. α is the channel gradient, α_1 is the theoretical boundary of the channel gradient between fully unsaturated and partly saturated sediment transport, and α_2 is the theoretical boundary of the channel gradient between partly and fully saturated sediment transport.**

7 Summary and conclusion

We investigated the interaction between flow characteristics and topography in the debris flow initiation zone at the Ohya

20 landslide, Japan, using various methods, including a physical analysis of static force, field monitoring, periodical TLS surveys, and an estimation of the volume of storage using GIS. Our study revealed that both partly and fully saturated debris flows are important hydrogeomorphic processes in the initiation zone because of the steep terrain. The predominant type of flow (partly or fully saturated) is affected by the volume of storage as well as rainfall patterns, which control the amount of water in the storage. In addition, small-scale channel gradients (on the order of meters) formed by erosion and deposition during debris

25 flow events reflect the dominant flow type in the flow. Such interactions between flow characteristics and topography could be explained by a simple analysis of static force at the bottom of the sediment mass.

Our study implies that the volume of storage and the rainfall patterns, which control predominant debris flow type classified by the ratio of the depth of the saturated zone, are potential information to improve debris-flow warning system, since the flow characteristics (e.g., sediment concentration, velocity) is different among debris flow types. In addition, our study elucidated that the slope gradient of geomorphic units is the key factor in the estimation of predominant type of the sediment transport

5   processes in debris flow torrents. Therefore periodical measurement of the topography in debris flow initiation zones is considered to be essential for the better risk assessment of debris-flow hazards.

10   **References**

Arattano, M.: On the use of seismic detectors as monitoring and warning system for debris flows, Nat. Hazards, 20, 197–213, 1999.

Arattano, M., Marchi, L., and Cavalli, M.: Analysis of debris-flow recordings in an instrumented basin: confirmations and new findings, Nat. Hazards Earth Syst. Sci, 12, 679–686, 2012.

15   Berger, C., McArdell, B. W., and Schlunegger, F.: Sediment transfer patterns at the Illgraben catchment, Switzerland: Implications for the time scales of debris flow activities, Geomorphology, 125, 421-432, 2011a.

Berger, C., McArdell, B. W., and Schlunegger, F.: Direct measurement of channel erosion by debris flows, Illgraben, Switzerland. J. Geophys. Res, 116, F01002, 2011b, doi:10.1029/2010JF001722

Berti, M., Genevois, R., Simoni, A., and Tecca, P. R.: Field observations of a debris flow event in the Dolomites,

20   Geomorphology, 29, 265–274, 1999.

Bovis M. J., and Jakob, M.: The roll of debris supply conditions in predicting debris flow activity, Earth Surf. Process. Landf., 24, 1039–1054, 1999.

Carson, M. A.: Angle of repose, angle of shearing resistance and angle of talus slopes, Earth Surf. Process,. 2, 368–380, 1977.

Chen, H. X., Zhang, L. M., Chang, D. S., and Zhang, S.: Mechanisms and runout characteristics of the rainfall triggered debris

25   flow in Xiaojiagou in Sichuan Province, China, Nat. Hazards, 62, 1037–1057, 2012.

Coussot, P., and Meunie, M.: Recognition, classification and mechanical description of debris flows, Earth-Sci. Rev., 40, 209–227, 1996.

Cui, P., Hu, K., Zhuang, J., Yang, Y., and Zhang, J.: Prediction of debris-flow danger area by combining hydrological and inundation simulation methods, J. Moun. Sci., 8, 1–9, 2011, doi: 10.1007/s11629-011-2040-8

30   Dorren, L. K. A.: A review of rockfall mechanics and modelling approaches, Prog. Phys. Geogr. 27, 1, 69–87, 2003.

Egashira, S., Itoh, T. and Takeuchi, H.: Transition mechanism of debris flows over rigid bed to over erodible bed, Phys. Chem. Earth, Part B: Hydrology, Oceans and Atmosphere, 26, 169–174, 2001, doi:10.1016/S1464-1909(00)00235-5

Gabet E. J.: Sediment transport by dry ravel, J. Geophys. Res., 108(B1), 2049, 2003, doi: 10.1029/2001JB001686

Hayakawa Y., Imaizumi, F., Hotta, N., and Tsunetaka, H.: Towards Long-Lasting Disaster Mitigation Following a Mega-landslide: High-Definition Topographic Measurements of Sediment Production by Debris Flows in a Steep Headwater Channel, In Geomorphology and Society, Springer, 2016.

Hu, K., Wei, F., and Li, Y.: Real-time measurement and preliminary analysis of debris-flow impact force at Jiangjia Ravine, China, Earth Surf. Process. Landf, 36, 1268–1278, 2011.

Hunger, O.: Classification and terminology, In Debris-flow Hazards and Related Phenomena, Praxis, Springer, Berlin Heidelberg, 106–134, 2005.

Hürlimann, M., Abancó, C., Moya, J., and Vilajosana, I.: Results and experiences gathered at the Rebaixader debris-flow monitoring site, Central Pyrenees, Spain, Landslides, 11, 939–953, 2014. doi: 10.1007/s10346-013-0452-y

Hürlimann, M., McArdell, B. W., and Rickli, C.: Field and laboratory analysis of the runout characteristics of hillslope debris flows in Switzerland, Geomorphology, 232, 20–32, 2015. doi:10.1016/j.geomorph.2014.11.030

Imaizumi, F., Tsuchiya, S., and Ohsaka, O.: Behaviour of debris flows located in a mountainous torrent on the Ohya landslide, Japan, Can. Geotech. J., 42, 919–931, 2005.

Imaizumi, F., Sidle, R. C., Tsuchiya, S., and Ohsaka, O.: Hydrogeomorphic processes in a steep debris flow initiation zone, Geophys. Res. Lett., 33, L10404, 2006.

Imaizumi, F., Nishii, R., Murakami, W., and Daimaru, H.: Parallel retreat of rock slopes underlain by alternation of strata, Geomorphology, 238, 27–36, 2015.

Imaizumi, F., Trappman, D., Matsuoka, N., Tsuchiya, S., Ohsaka, O. and Stoffel, M.: Biographical sketch of a giant: deciphering recent debris-flow dynamics from Ohya landslide body (Japanese Alps), Geomorphology, 272, 102–114, 2016a, http://dx.doi.org/10.1016/j.geomorph.2015.11.008

Imaizumi, F., Tsuchiya, S., and Ohsaka, O.: Behavior of boulders within a debris flow initiation zone, Int. J. Erosion Control Eng., 9(3), 91-100, 2016b, doi:http://doi.org/10.13101/ijece.9.91

Imaizumi F., Tsuchiya, S., and Ohsaka, O.: Field observations of debris-flow initiation processes on sediment deposits in a previous deep-seated landslide site, J. Mount. Sci, 13, 213–222, 2016c, doi: 10.1007/s11629-015-3345-9

Jakob, M., Bovis, M., and Oden, M.: The significance of channel recharge rates for estimating debris-flow magnitude and frequency, Earth Surf. Process. Landf., 30, 755–766, 2005.

Kean, J. W., McCoy, S. W., Tucker, G. E., Staley, D. M., and Coe, J. A.: Runoff-generated debris flows: Observations and modeling of surge initiation, magnitude, and frequency, J. Geophys. Res, 18, 2190–2207, 2013, doi:10.1002/jgrf.20148

Kirkby, M. J., and Statham, I.: Surface stone movement and scree formation, J. Geology, 83, 349–362, 1975.

Lin, P. S., Lin, J. Y., Hung, J. C., and Yang, M. D.: Assessing debris-flow hazard in a watershed in Taiwan, Eng. Geol., 66, 295–313, 2002,doi: 10.1016/S0013-7952(02)00105-9

March, L., Arattano, M., and Deganutti, A. M.: Ten years of debris-flow monitoring in the Morcardo Torrent (Italian Alps), Geomorphology, 46, 1–17, 2002.

Mangeney, A., Bouchut, F., Thomas, N., Vilotte, J. P., and Bristeau, M. O.: Numerical modeling of self-channeling granular flows and of their levee-channel deposits, J. Geophys. Res, 112, F02017, 2007, doi:10.1029/2006JF000469

5 McArdell, B. W., Bartelt, P., and Kowalski, J.: Field observations of basal forces and fluid pore pressure in a debris flow, Geophys. Res Lett., 34, L07406, 2007, doi:10.1029/2006GL029183

McCoy, S. W., Kean, J. W., Coe, J. A., Staley, D. M., Wasklewicz, T. A., and Tucker, G. E.: Evolution of a natural debris flow: In situ measurements of flow dynamics, video imagery, and terrestrial laser scanning, Geology, 38, 735–738, 2010.

McCoy, S. W., Kean, J. W., Coe, J. A., Tucker, G. E., Staley, D. M., and Wasklewicz, T. A.: Sediment entrainment by debris

10 flows: In situ measurements from the headwaters of a steep catchment, J. Geophys. Res., 117, F03016, 2012, doi:10.1029/2011JF002278

McCoy, S.W., Tucker, G. E., Kean, J. W., and Coe, J. A.: Field measurement of basal forces generated by erosive debris flows, J. Geophys. Res, 118, 589–602, 2013, doi:10.1002/jgrf.20041.

Navratil, O., Liébault, F., Bellot, H., Travaglini, E., Theule, J., Chambon, G., and Laigle, D.: High-frequency monitoring of

15 debris-flow propagation along the Réal Torrent, Southern French Prealps, Geomorphology, 201, 157–171, 2013.

Obanawa, H., Matsukura, Y.: Cliff retreat and talus development at the caldera wall of Mount St. Helens: Computer simulation using a mathematical model, Geomorphology, 97, 697–711, 2008.

Okano, K., Suwa, H., and Kanno T.: Characterization of debris flows by rainstorm condition at a torrent on the Mount Yakedake volcano, Japan, Geomorphology, 136, 88–94, 2012.

20 Pareschi, M. T., Santacroce, R., Sulpizio, R., and Zanchetta, G.: Volcaniclastic debris flows in the Clanio Vally (Campania, Italy): insights for the assessment of hazard potential, Geomorphology, 43, 219–231, 2002.

Schlunegger, F., Badoux, A., McArdell, B. W., Gwerder, C., Schnydrig, D., Rieke-Zapp, D., and Molnar, P.: Limits of sediment transfer in an alpine debris-flow catchment, Illgraben, Switzerland, Quat. Sci. Rev., 28, 1097–1105, 2009.

Staley, D. N., Wasklewicz, T. A., and Blaszczynsk, J. S.: Surficial patterns of debris flow deposition on alluvial fans in Death

25 Valley, CA using airborne laser swath mapping data, Geomorphology, 74, 152–163, 2006.

Takahashi, T.: An occurrence mechanism of mud-debris flows, and their characteristics in motion. Annuals, DPRI, 23B2, 405–435 (in Japanese), 1977.

Takahashi, T: Debris flow, IAHR Monograph. A.A. Balkema, Rotterdam, 1991.

Takahashi, T.: Debris flow, CRC Press/Balkema, EH Leiden, Netherlands, 2014.

30 Takahashi, T., and Tsujimoto, H.: A mechanical model for Merapi-type pyroclastic flow, J. Volcanol. Geotherm. Res., 98, 91–115, 2000, doi:10.1016/S0377-0273(99)00193-6

Tsuchiya, S., and Imaizumi, F.: Large sediment movement caused by the catastrophic Ohya-kuzure landslide, J. Dis. Sci., 3(5), 257–263, 2010.

VanDine, D. F.: Debris flows and debris torrents in the southern Canadian Cordillera, Can. Geotech. J., 22, 44–62, 1985.

Whipple K. X., and Dunne, T.: The influence of debris-flow rheology on fan morphology, Owens Valley, California, Geol. Soc. Am. Bull., 104, 887–900, 1992.

Watanabe, S.: Influence of the mixing ratio of water to sediment on the threshold slope of debris flow: a laboratory experiment, Trans. Jpn. Geomorph. Union, 15, 349–369 (in Japanese with English abstract), 1994.

5 Yamashita, S., and Miyamoto, K.: Sediment Problems: Strategies for Monitoring, Prediction and Control (Proceedings of the Yokohama Symposium), IAHS Publ. no. 217, 67–74, 1993.

Zhang, S.: A comprehensive approach to the observation and prevention of debris flows in China, Nat. Hazards, 7, 1–23, 1993.